**Acknowledgment.** Work performed at Iowa State University (R.A.N., D.S.M.) was supported by NSF Grants CHE76-83665 and CHE80-00744; we are indebted to Professor R. A. Jacobson, who provided the X-ray diffraction equipment. Research at the California Institute of Technology (A.E.S., C.-M.C., W.P.S., V.M.M., H.B.G.) was supported by the Office of Naval Research and the National Science Foundation. Portions of this work (R.F.D., W.H.W.) were performed at Los Alamos National Laboratory under the auspices of the U.S. Department of Energy.

**Registry No.** $K_2[Pt_2(SO_4)_4(OH_2)_2]$, 70085-58-4; $K_4[Pt_2(SO_4)_4Cl_2]$, 58807-44-6; $Cs_4[Pt_2(SO_4)_4Br_2]$, 60910-61-4; $K_2[Pt_2(SO_4)_4(DMSO)_2]\cdot 4H_2O$, 81602-75-7.

Contribution from the Department of Chemistry and Biochemistry, University of Notre Dame, Notre Dame, Indiana 46556

# Spectroscopic and Electrochemical Characterization of Nickel β-Oxoporphyrins: Identification of Nickel(III) Oxidation Products

Patricia A. Connick and Kathleen A. Macor*

*Received October 12, 1990*

Seven nickel di- and tri-β-oxoporphyrins ([3,3,7,8,12,13,17,17-octaethyl-2,18(3*H*,17*H*)-porphinedionato(2-)]nickel, [3,3,8,8,12,13,17,18-octaethyl-2,7(3*H*,8*H*)-porphinedionato(2-)]nickel (NiDP-II), [3,3,7,7,12,13,17,18-octaethyl-2,8(3*H*,7*H*)-porphinedionato(2-)]nickel, [3,3,7,8,12,12,17,18-octaethyl-2,13(3*H*,12*H*)-porphinedionato(2-)]nickel, [3,3,7,8,13,13,17,18-octaethyl-2,12(3*H*,13*H*)-porphinedionato(2-)]nickel, [3,3,7,8,12,12,18,18-octaethyl-2,13,17(3*H*,12*H*,18*H*)-porphinetrionato(2-)]nickel (NiTP-A), and [3,3,8,8,13,13,17,18-octaethyl-2,7,12(3*H*,8*H*,13*H*)-porphinetrionato(2-)]nickel) were prepared by hydrogen peroxide oxidation of octaethylporphyrin followed by metalation. These compounds and the previously synthesized nickel mono-β-oxoporphyrin [3,3,7,8,12,13,17,18-octaethyl-2(3*H*)-porphinonato(2-)]nickel (NiMP) (Stolzenberg, A. M.; Glazer, P. A.; Foxman, B. M. *Inorg. Chem.* **1986**, *25*, 983-991) were characterized by electronic absorption spectroscopy, $^1H$ NMR spectroscopy, resonance Raman (RR) spectroscopy, and cyclic voltammetry. EPR spectra of the one-electron-oxidation products of NiMP, NiDP-II, and NiTP-A in methylene chloride and acetonitrile have also been obtained. A solvent-induced switch in the site of one-electron abstraction occurs in NiDP-II, where a $Ni^{III}$DP-II series is produced in acetonitrile solution and a $Ni^{II}$DP-II cation radical is generated in methylene chloride solution. In both solvents one-electron oxidation of NiMP yields a $Ni^{II}$MP cation radical while one-electron oxidation of NiTP-A yields $Ni^{III}$TP-A species. EPR signals from the Ni(III) centers ($g_{av}$ = 2.24) are observed at liquid-nitrogen temperature. This is the first report of the Ni(III) state in a porphyrinic derivative at room temperature. The $Ni^{3+/2+}$ potential for NiTP-A is 0.34 V (vs SCE), which is one of the lowest reported for this redox couple. We suggest that stabilization of Ni(III) by the β-oxoporphyrins is based on a balance of π-conjugation, ring ruffling, and axial ligation. The nickel β-oxoporphyrins exhibit a greater number of Raman bands than nickel octaethylporphyrin (NiOEP) due to their lower symmetry. Vibrational modes that are only IR-active in NiOEP ($D_{4h}$ symmetry) are observed with strong intensities in the Raman spectra of the nickel β-oxoporphyrins, which are best described as having $C_2$ symmetry. A carbonyl stretching mode in the 1708-1716-$cm^{-1}$ region is observed as one of the strongest bands in the RR spectrum of each nickel β-oxoporphyrin, and is an identifying feature of the β-oxoporphyrin spectra.

## Introduction

Nature uses a variety of porphyrinic ligands to bind metal ions in enzymes. Examples are the ubiquitous porphyrin ring, which binds iron in such proteins as hemoglobin,[1] myoglobin,[1] peroxidases,[2] and cytochromes,[3] the Co corrin ring of coenzyme $B_{12}$,[4] the corphin ring of methylreductase $F_{430}$ from methanogenic bacteria, which binds nickel,[5] the iron isobacteriochlorin ring of sulfite reductase siroheme,[6] and the di-β-oxoporphyrin ring[7] of dissimilatory nitrite reductase heme $d_1$, which binds iron.[8] The corphin and corrin rings of methylreductase $F_{430}$ and coenzyme $B_{12}$, respectively, appear to have been chosen for their flexibility, which modulates Co-C bond cleavage in coenzyme $B_{12}$[9] and axial ligation[10] and possibly redox properties[11] of the Ni center in methylreductase $F_{430}$. Crystal structures of the enzymes have shown that the corrin[12] and corphin[13] rings are considerably more ruffled than the porphyrin rings in hemoglobin and myoglobin, for example.[14] This trend has also been demonstrated with nonprotein bound corphins[10b] and porphyrins.[15]

We are interested in understanding the role that the di-β-oxoporphyrin-II ring (structure **4** in Figure 1)[8] plays in the chemistry of dissimilatory nitrite reductase heme $d_1$. The enzyme functions in a redox capacity accepting reducing equivalents from donor c-type cytochromes and transfers these to nitrite, reducing it to nitric oxide. It consists of a dimer whose subunits each contain two hemes, one type c and the other type $d_1$.[16]

Although di-β-oxoporphyrin ring oxidation potentials are similar to those of porphyrins[17,18] their $Fe^{3+/2+}$ potentials are approximately 0.25 V more positive than those of porphyrins.[17] In contrast, $Fe^{3+/2+}$ potentials vary by less than 0.10 V from iron isobacteriochlorin and iron chlorin to iron porphyrin.[19] These data indicate that the di-β-oxoporphyrin ring modulates bound

* To whom correspondence should be addressed.

(1) Ten Eyck, L. F. In *The Porphyrins*; Dolphin, D., Ed.; Academic Press: New York, 1979; Vol. VII, Chapter 10.
(2) Hewson, W. D.; Hager, L. P. In *The Porphyrins*; Dolphin, D., Ed.; Academic Press: New York, 1979; Vol. VII, Chapter 6.
(3) (a) Ortiz de Montellano, P. R. *Acc. Chem. Res.* **1987**, *20*, 289-294. (b) Wilson, D. F.; Erecinska, M. In *The Porphyrins*; Dolphin, D., Ed.; Academic Press: New York, 1979; Vol. VII, Chapter 1. (c) Cramer, W. A.; Whitmarsh, J.; Horton, P. In *The Porphyrins*; Dolphin, D., Ed.; Academic Press: New York, 1979; Vol. VII, Chapter 2. (d) Timkovich, R. S. In *The Porphyrins*; Dolphin, D., Ed.; Academic Press: New York, 1979; Vol. VII, Chapter 5.
(4) Golding, B. T. In $B_{12}$; Dolphin, D., Ed.; Wiley: New York, 1982; Vol. 1, Chapter 15.
(5) Pfaltz, A. In *The Bioinorganic Chemistry of Nickel*; Lancaster, J. R., Ed.; VCH Publishers: New York, 1988; Chapter 12.
(6) Siegel, L. M. *Dev. Biochem.* **1978**, *1*, 201-214.
(7) Abbreviations and numbering scheme are as follows: NiMP (nickel mono-β-oxoporphyrin, **2b**), [3,3,7,8,12,13,17,18-octaethyl-2(3*H*)-porphinonato(2-)] nickel; NiDP-I (nickel di-β-oxoporphyrin-I, **3b**), [3,3,7,8,12,13,17,17-octaethyl-2,18(3*H*,17*H*)-porphinedionato(2-) nickel; NiDP-II (nickel di-β-oxoporphyrin-II, **4b**), [3,3,8,8,12,13,17,18-octaethyl-2,7(3*H*,8*H*)-porphinedionato(2-) nickel; NiDP-III (nickel di-β-oxoporphyrin-III, **5b**), [3,3,7,7,12,13,17,18-octaethyl-2,8(3*H*,7*H*)-porphinedionato(2-) nickel; NiDP-IV (nickel di-β-oxoporphyrin-IV, **6b**), [3,3,7,8,12,12,17,18-octaethyl-2,13-(3*H*,12*H*)-porphinedionato(2-) nickel; NiDP-V (nickel di-β-oxoporphyrin-V, **7b**), [3,3,7,8,13,13,17,18-octaethyl-2,12(3*H*,13*H*)-porphinedionato(2-) nickel; NiTP-A (nickel tri-β-oxoporphyrin-A, **8b**), [3,3,7,8,12,12,18,18-octaethyl-2,13,17(3*H*,12*H*,18*H*)-porphinetrionato-(2-) nickel; NiTP-B (nickel tri-β-oxoporphyrin-B, **9b**), [3,3,8,8,13,13,17,18-octaethyl-2,7,12(3*H*,8*H*,13*H*)-porphinetrionato(2-) nickel.
(8) Chang, C. K. *J. Biol. Chem.* **1985**, *260*, 9520-9522.
(9) (a) Geno, M. K.; Halpern, J. *J. Am. Chem. Soc.* **1987**, *109*, 1238-1240. (b) Babior, B. M. In $B_{12}$; Dolphin, D., Ed.; Wiley: New York, 1982; Vol. 2, Chapter 10.

0020-1669/91/1330-4654$02.50/0 

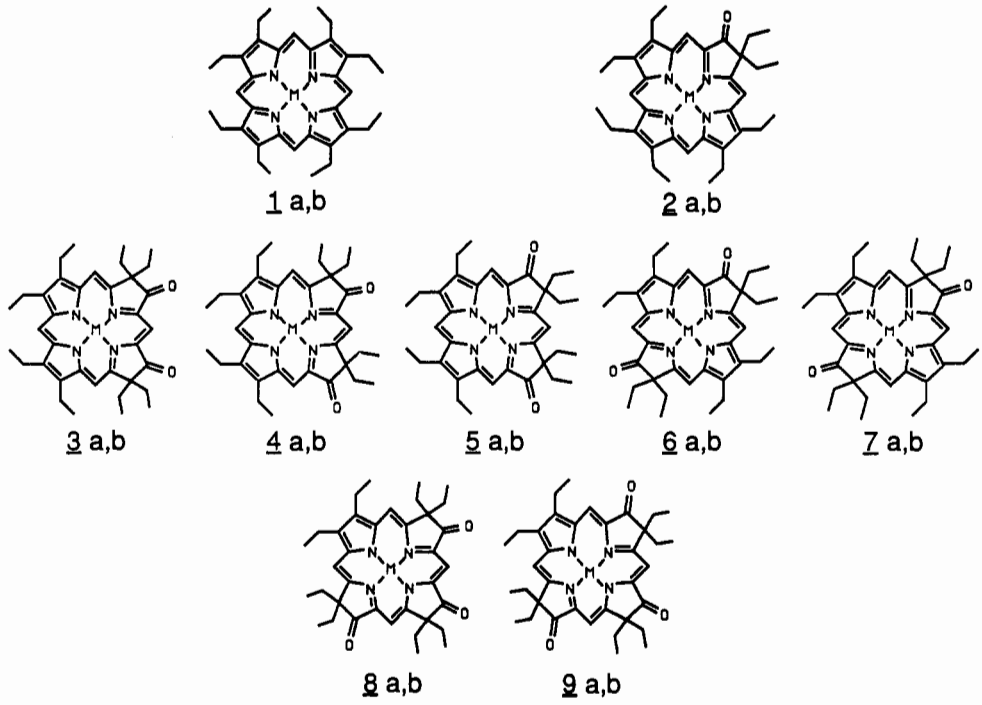


**Figure 1.** Structures of NiOEP and β-oxoporphyrins (compound a, M = 2H; compound b, M = Ni).

metal redox chemistry to a greater extent than other porphyrinic ligands.

We have prepared nickel complexes of mono-β-oxoporphyrin (NiMP), the five isomeric di-β-oxoporphyrins (NiDP), and two of the isomeric tri-β-oxoporphyrins (NiTP) in order to carry out a comprehensive examination of the spectroscopic and oxidative electrochemical characteristics of this class of porphyrins. Cyclic voltammograms of each compound have been analyzed in methylene chloride and acetonitrile solutions. EPR spectra of the one-electron-oxidation products of NiMP, NiDP-II, and NiTP-A in methylene chloride and acetonitrile have also been obtained. A solvent-induced switch in the site of one-electron abstraction occurs in NiDP-II, whereas a $Ni^{III}$DP-II species is produced in acetonitrile solution and a $Ni^{II}$DP-II cation radical is generated in methylene chloride solution. In both solvents, one-electron oxidation of NiMP yields a $Ni^{II}$MP cation radical while one-electron oxidation of NiTP-A yields $Ni^{III}$TP-A species. EPR signals from the Ni(III) centers ($g_{av}$ = 2.24) are observed at liquid-nitrogen temperature. NiDP-II and NiTP-A are the first unambiguous examples of porphyrinic compounds that stabilize Ni(III) at room temperature. $Ni^{III}$TPP has been formed at liquid-nitrogen temperature,[20] and $Ni^{III}$OEC$^{\bullet+}$ and $Ni^{III}$OEiBC$^{\bullet+}$ have been postulated on the basis of solvent-dependent redox potentials and electronic absorption data.[21] The $Ni^{3+/2+}$ potential of NiTP-A (0.34 V vs SCE) is nearly 0.8 V lower than that of NiTPP and is one of the lowest reported for this redox couple with any ligand.[22]

We suggest that the di- and tri-β-oxoporphyrin rings have a greater tendency to stabilize Ni(III) than the porphyrin ring due to the greater tendency of the former compounds to bind axial ligands and relieve the strain of ruffling. Recent X-ray crystallographic data[23] show that NiDP-II and NiTP-A are nearly as ruffled as chlorins with average methine carbon deviations from the plane of the four nitrogens of 0.45 and 0.51 Å, respectively. Axial ligation could raise the energy of the Ni $d_{z^2}$ orbital above the β-oxoporphyrin π orbitals, which could lead to a Ni-centered highest-occupied orbital (HOMO) in the β-oxoporphyrins. In Ni chlorins and isobacteriochlorins the Ni $d_{z^2}$ orbital cannot rise above the chlorin or isobacteriochlorin π orbitals because the latter are at considerably higher energies due to the lower aromaticity of the chlorin and isobacteriochlorin rings. The balance of π-conjugation, ring ruffling, and axial ligation apparently achieved by the β-oxooctaethylporphyrins facilitates at least one example of metal redox chemistry that is inaccessible to other classes of octaethylporphyrinic ligands.

We have also analyzed the resonance Raman spectra of NiMP, the five isomeric NiDP's, and one NiTP isomer. The Raman bands have been identified by using established assignments for NiOEP,[24] nickel octaethylchlorin (NiOEc),[25] and nickel octaethylisobacteriochlorin (NiOEiBC)[26] as references. We have found that β-oxoporphyrins exhibit a greater number of Raman bands than NiOEP due to their lowered symmetry. Vibrational modes that were only IR-active in NiOEP ($D_{4h}$ symmetry)[24] are observed with strong intensities in the Raman spectra of the nickel β-oxoporphyrins, which are best described as having $C_2$ symmetry. A strongly enhanced carbonyl stretching mode is seen in the

(10) (a) Eschenmoser, A. *Ann. N.Y. Acad. Sci.* **1986**, *471*, 108–123. (b) Kratky, C.; Waditschatka, R.; Angst, C.; Johansen, J. E.; Plaquevent, J. C.; Schreiber, J.; Eschenmoser, A. *Helv. Chim. Acta* **1985**, *68*, 1312–1337. (c) Pfaltz, A.; Livingston, D. A.; Jaun, B.; Diekert, G.; Thauer, R. K.; Eschenmoser, A. *Helv. Chim. Acta* **1985**, *68*, 1338–1358.
(11) Jaun, B.; Pfaltz, A. *J. Chem. Soc., Chem. Commun.* **1986**, 1327–1329.
(12) Glusker, J. In $B_{12}$; Dolphin, D., Ed.; Wiley: New York, 1982; Vol. 1, Chapter 3.
(13) Pfaltz, A.; Jaun, B.; Fassler, A.; Eschenmoser, A.; Jaenchen, R.; Gilles, H. H.; Diekert, G.; Thauer, R. K. *Helv. Chim. Acta* **1982**, *65*, 828–832.
(14) (a) Muirhead, H.; Greer, J. *Nature* **1970**, *228*, 516–519. (b) Kendrew, J. C.; Dickerson, R. E.; Strandberg, B. E.; Hart, R. G.; Davies, D. R.; Phillips, D. C.; Shore, V. C. *Nature* **1960**, *185*, 422–426.
(15) Scheidt, W. R.; Lee, Y. J. *Struct. Bonding* **1987**, *64*, 1–70.
(16) Kuronen, T.; Ellfolk, N. *Biochim. Biophys. Acta* **1972**, *275*, 308–318.
(17) Chang, C. K.; Barkigia, K. M.; Hanson, L. K.; Fajer, J. *J. Am. Chem. Soc.* **1986**, *108*, 1352–1354.
(18) Stolzenberg, A. M.; Glazer, P. A.; Foxman, B. M. *Inorg. Chem.* **1986**, *25*, 983–991.
(19) Stolzenberg, A. M.; Strauss, S. H.; Holm, R. H. *J. Am. Chem. Soc.* **1981**, *103*, 4763–4778.
(20) (a) Dolphin, D.; Niem, T.; Felton, R. H.; Fujita, I. *J. Am. Chem. Soc.* **1975**, *97*, 5288–5290. (b) Wolberg, A.; Manassen, J. *J. Am. Chem. Soc.* **1970**, *92*, 2982–2984.
(21) Stolzenberg, A. M.; Stershic, M. T. *Inorg. Chem.* **1988**, *27*, 1614–1620.
(22) Lappin, A. G.; McAuley, A. *Adv. Inorg. Chem.* **1988**, *32*, 241–295.
(23) Connick, P. A.; Haller, K. J.; Macor, K. A. Manuscript in preparation.
(24) Li, X. Y.; Czernuszewicz, R. S.; Kincaid, J. R.; Stein, P.; Spiro, T. G. *J. Phys. Chem.* **1990**, *94*, 47–61.
(25) (a) Prendergast, K.; Spiro, T. G. *J. Phys. Chem.* **1991**, *95*, 1555–1563. (b) Boldt, N. J.; Donohoe, R. J.; Birge, R. R.; Bocian, D. F. *J. Am. Chem. Soc.* **1987**, *109*, 2284–2298.
(26) Melamed, D.; Sullivan, E. P.; Prendergast, K.; Strauss, S. H.; Spiro, T. G. *Inorg. Chem.* **1991**, *30*, 1308–1319.

1705–1720-cm$^{-1}$ region of the spectrum of each nickel β-oxoporphyrin. Similar bands have been reported in the resonance Raman spectra of copper di-β-oxoporphyrins[27] and intact heme $d_1$.[28]

## Experimental Section

**Chemicals.** $H_2OEP$, NiOEP, and MgOEP (Mid-Century Chemicals, Posen, IL) were shown to be pure by thin-layer chromatography (TLC) on alumina basic plates and used as received. Tetrabutylammonium perchlorate (TBAP) (GFS Chemicals, Columbus, OH) was recrystallized from ethyl acetate and dried in vacuo. N,N-dimethylformamide (DMF) (Fisher, Pittsburgh, PA) and $CH_2Cl_2$ (Fisher, Pittsburgh, PA) were dried over $CaH_2$ and distilled prior to use. Methanol (Fisher, Pittsburgh, PA) was dried over anhydrous $Na_2SO_4$, and spectrophotometric grade acetonitrile (Aldrich, Milwaukee, WI) was used as received. Analtech (Newark, DE) thin-layer silica gel G (250 and 1000 μm) and Woelm alumina basic and acidic (250 μm) plates were used for chromatographic separations. The NMR solvents, $CDCl_3$, and $CD_3CN$ (>99.5 atom % D; Aldrich, Milwaukee, WI), were used as received.

**Preparation of Free-Base β-Oxoporphyrins.** Oxidation of $H_2OEP$ with $H_2O_2$ in concentrated $H_2SO_4$ was accomplished by literature methods[18,29,30] on approximately 100-mg batches. Because of the small amount of starting material, TLC rather than column chromatography was used to achieve separation of the reaction products. Each crude reaction mixture was separated on 10 × 20 cm 1000 μm silica gel plates using 4:1 methylene chloride/hexane as solvent. The following is the order of development (in order of decreasing $R_f$ values): **10a**,[31] **1a**, **2a**, **7a** with **5a** and **6a**, **4a** with **9a**, and **3a** with **8a**. Approximately half of the crude reaction mixture remained as a dark brown residue at the bottom of the plates. Bands were sliced from the plates, the compounds were extracted with methylene chloride followed by methanol, and the solvent was evaporated under vacuum. NMR spectroscopy was used to determine the purity of each compound. Our product distributions were more similar to those of Inhoffen and Nolte[29] than those of Chang.[30a] As in Stolzenberg's work[18] a small amount (approximately 3%) of the meso-oxidation product, α,γ-dioxoporphodimethene, was isolated.

**6a** was separated from **5a** and **7a** by rechromatographing with pure methylene chloride on 250 μm silica gel plates. Separation of **7a** from **5a** was then accomplished with a 3:2 methylene chloride/hexane solvent mix using 250 μm alumina basic plates. Separation of **3a** and **8a** required an 80:1 mix of methylene chloride/methanol on 250 μm silica gel plates. **4a** and **9a** could not be separated as free bases and so were separated after insertion of the nickel (see below).

**Preparation of Nickel β-Oxoporphyrins by Individual Metalations.** Insertion of nickel into each of the separated free-base compounds was accomplished by the method of Adler[32] using $NiCl_2{\cdot}6H_2O$ in DMF in a 15:1 mole ratio of nickel to porphyrin. Most free-base oxoporphyrins required 3 h or less refluxing time for complete metalation to occur (as determined by the electronic absorption spectrum). However, **6a** and **7a** could not be completely metalated even after 12 h of refluxing. In general, the process of metalation seems to involve some reduction of the β-oxoporphyrin. (For example, the insertion of metal into **2a** formed not only **2b** but also a small amount of **1b**.) Products were identified by their characteristic electronic absorption and NMR spectra. Relative extinction coefficients based on peak heights are listed below for each nickel compound (in methylene chloride) along with details of the separation procedure.

**(a) Isolation of 2b.** The nickel compound **2b** was separated from the unreacted free-base counterpart **2a** and **1b** by using a 4:1 methylene chloride/hexane mix on 250 μm silica gel plates. The electronic absorption spectrum was consistent with that reported by Stolzenburg.[18] UV–vis [$\lambda_{max}$, nm ($A_\lambda/A_{413}$)]: 372 s (0.43), 413 (1.00), 506 (0.05), 545 (0.07), 571 (0.10), 616 (0.56). (See inset, Figure 5.) $^1$H NMR ($CDCl_3$), δ: 0.44 (t, gem $CH_3$); 1.65, 1.67, 1.70 (×2), 1.73, 1.74 (t, $CH_3$); 2.55 (m, gem $CH_2$); 3.65, 3.71, 3.75 (×4) (q, $CH_2$); 8.56, 9.30, 9.37, 9.44 (s, meso H). A low-resolution mass spectrum showed a peak at *m/e* 606.

**(b) Isolation of 3b.** A 4:1 methylene chloride/hexane solvent mixture on 250 μm alumina basic plates was used to isolate **3b**. UV–vis [$\lambda_{max}$, nm ($A_\lambda/A_{429}$)]: 402 s (0.84), 429 (1.00), 536 (0.09), 573 (0.15), 648 s (0.13), 699 (0.93). (See inset, Figure 5.) $^1$H NMR ($CDCl_3$), δ: 0.45 (t, gem $CH_3$); 1.60, 1.67 (t, $CH_3$); 2.44 (m, gem $CH_2$); 3.55, 3.65 (q, $CH_2$); 8.36 (×2), 8.91, 9.20 (s, meso H). A low-resolution mass spectrum showed a peak at *m/e* 622.

**(c) Isolation of 4b.** Because **4a** and **9a** were not separable they were simultaneously metalated. Metalation was complete and the nickel species, **4b** and **9b**, were separable under conditions identical with those used to isolate **3b**. UV–vis [$\lambda_{max}$, nm ($A_\lambda/A_{438}$) (for **4b**)]: 388 (0.99), 438 (1.00), 586 s (0.30), 621 (0.99). (See inset, Figure 4.) $^1$H NMR ($CDCl_3$), δ: 0.39, 0.48 (t, gem $CH_3$); 1.53, 1.56, 1.61, 1.62 (t, $CH_3$); 2.39 (m, gem $CH_2$); 3.44, 3.50, 3.54, 3.55 (q, $CH_2$); 8.08, 8.09, 8.90, 8.99 (s, meso H).

**(d) Isolation of 5b.** This product was synthesized only under conditions of batch metalation (see below). UV–vis [$\lambda_{max}$, nm ($A_\lambda/A_{409}$)]: 370 s (0.52), 409 (1.00), 503 (0.07), 534 (0.08), 595 (0.17), 648 (0.93). $^1$H NMR ($CDCl_3$), δ: 0.46 (t, gem $CH_3$); 1.5, 1.6 (t, $CH_3$); 2.34 (m, gem $CH_2$); 3.43, 3.48 (q, $CH_2$); 7.40, 8.73 (×2), 8.90 (s, meso H).

**(e) Isolation of 6b.** Separation was accomplished under conditions identical with those used to isolate **2b**. UV–vis [$\lambda_{max}$, nm ($A_\lambda/A_{438}$)]: 375 (0.60), 420 s (0.63), 438 (1.00), 545 (0.08), 584 (0.21), 675 (0.67). (See inset, Figure 6.) $^1$H NMR ($CDCl_3$), δ: 0.47 (t, gem $CH_3$); 1.58, 1.62 (t, $CH_3$); 2.45 (m, gem $CH_2$); 3.52, 3.54 (q, $CH_2$); 8.29, 9.03 (s, meso H).

**(f) Isolation of 7b.** Separation was accomplished under conditions identical with those used to isolate **2b**. UV–vis [$\lambda_{max}$, nm ($A_\lambda/A_{419}$)]: 377 (0.54), 419 (1.00), 513 (0.06), 551 (0.05), 651 (0.10), 671 (0.18), 706 (1.27). $^1$H NMR ($CDCl_3$), δ: 0.46 (t, gem $CH_3$); 1.62, 1.63 (t, $CH_3$); 2.48 (m, gem $CH_2$); 3.57, 3.62 (q, $CH_2$); 8.45, 9.15 (s, meso H).

**(g) Isolation of 8b.** Separation was accomplished under conditions identical with those used to isolate **3b**. UV–vis [$\lambda_{max}$, nm ($A_\lambda/A_{431}$)]: 357 (0.56), 431 (1.00), 471 s (0.40), 626 s (0.20), 652 s (0.36), 666 s (0.46), 680 (0.56), 732 (1.87). $^1$H NMR ($CDCl_3$), δ: 0.38, 0.48 (×2) (t, gem $CH_3$); 1.55, 1.56 (t, $CH_3$); 2.35 (m, gem $CH_2$); 3.43, 3.44 (q, $CH_2$); 8.03, 8.13, 8.15, 8.67 (s, meso H).

**(h) Isolation of 9b.** Separation was accomplished under conditions identical with those used to isolate **3b**. UV–vis [$\lambda_{max}$, nm ($A_\lambda/A_{427}$)]: 427 (1.00), 628 s (0.24), 667 (0.33), 7.16 (1.06). $^1$H NMR ($CDCl_3$), δ: 0.39, 0.40, 0.51 (t, gem $CH_3$); 1.49, 1.51 (t, $CH_3$); 2.32 (m, gem $CH_2$); 3.35, 3.42 (q, $CH_2$); 7.89, 7.94, 7.96, 8.75 (s, meso H).

**Preparation of Nickel β-Oxoporphyrins by Batch Metalations.** Oxidation of $H_2OEP$ was accomplished as above, but on approximately 200-mg batches. Nickel was inserted into the entire batch simultaneously by metalating for 3 h using the procedure outlined above. Because of the small amount of starting material, thin-layer rather than column chromatography was used to achieve separation of the reaction products. Each crude reaction mixture was separated on 10 × 20 cm 1000 μm silica gel plates by using 4:1 methylene chloride/hexane as solvent. The following is the order of development (in order of decreasing $R_f$ values with the colors of the bands on the plates/in solution given in parentheses): **1b** (red/pink), **10** b (brown/brown)[31] with an unidentifiable compound, **2b** (green/green), **7a** (slate blue/purple), **7b** (greenish brown/golden brown) with **6b** (green/green) and **5b** (green/green) and **6a**, **4b** (green/green), and **9b** (dark green/green) with **3b** (brown/greenish brown) and **8b** (bright green/bright green). The distribution of products was the same as for the oxidation reaction. However, because nickel was not easily inserted into **6a** and **7a**, only small amounts of **6b** and **7b** were formed. Approximately half of the crude reaction mixture remained as a dark brown residue at the bottom of the plates.

**(a) Isolation of 3b and 9b.** Isolation of both **3b** and **9b** was accomplished by chromatographing the mix of **3b**, **8b**, and **9b** on 250 μm silica gel plates using an 80:1 mix of methylene chloride/methanol as the solvent.

**(b) Isolation of 4b.** At times, **4b** was contaminated with **6b**. In these cases, a separation was achieved by chromatographing the mix on 250 μm silica gel plates using pure methylene chloride.

**(c) Isolation of 5b.** The mix of **5b**, **6a**, **6b**, and **7b** was chromatographed on 250 μm acidic alumina plates using a 60:40 mix of methylene chloride/hexane. The green band (predominantly **5b**) was rechromatographed on 250 μm silica gel plates using a 4:1 mix of methylene chloride/hexane.

**(d) Isolation of 6b.** The mix of **6b**, **5b**, **6a**, and **7b** was chromatographed on 250 μm silica gel plates using pure methylene chloride. The second green band (predominantly **6b**) was rechromatographed on 250 μm alumina acidic plates by using a 60:40 mix of methylene chloride and hexanes.

**(e) Isolation of 7b.** Because the small amount of **7b** present in the batch metalation could not be successfully isolated, nickel was inserted

(27) Andersson, L. A.; Loehr, T. M.; Wu, W.; Chang, C. K.; Timkovich, R. *FEBS Lett.* **1990**, *267*, 285–288.
(28) (a) Ching, Y.; Ondrias, M. R.; Rousseau, D. L.; Muhoberac, B. B.; Wharton, D. C. *FEBS Lett.* **1982**, *138*, 239–244. (b) Cotton, T. M.; Timkovich, R.; Cork, M. S. *FEBS Lett.* **1981**, *133*, 39–44.
(29) Inhoffen, H. H.; Nolte, W. *Liebigs Ann. Chem.* **1969**, *725*, 167–176.
(30) (a) Chang, C. K. *Biochemistry* **1980**, *19*, 1971–1976. (b) Bonnett, R.; Dimsdale, M. J.; Stephenson, G. F. *J. Chem. Soc. C* **1969**, 562–570.
(31) Compound **10a** is α,γ-dioxoporphodimethene; compound **10b** is nickel α,γ-dioxoporphodimethene.
(32) Adler, A. D.; Longo, F. R.; Kampas, F.; Kim, J. *J. Inorg. Nucl. Chem.* **1970**, *32*, 2443–2445.

separately into the pure band containing **7a** by using a 5-h reflux with a 50:1 nickel to porphyrin ratio. The reaction mix was chromatographed on 250 μm silica gel plates using 4:1 methylene chloride/hexane.

**(f) Isolation of 8b.** The second dark green band from the isolation of **3b** and **9b** was rechromatographed on 250 μm silica gel plates using a 97.5:2.5 mix of methylene chloride/methanol to yield **8b**.

**Electronic Absorption, NMR, and Mass Spectra.** Electronic absorption spectra (350–900 nm) were recorded on Beckman DU-40 and Varian DMS100 spectrophotometers. A General Electric 300-MHz spectrometer was used to obtain the NMR spectra. Chemical shifts are reported relative to $CHCl_3$ at 7.26 ppm or $CHD_2CN$ at 1.93 ppm. Mass spectra were recorded on a Finnegan MAT Model 8430 mass spectrometer using fast atom bombardment (FAB) with *m*-nitrobenzyl alcohol as solvent.

**EPR Spectra of Oxidized Compounds.** Oxidized samples were prepared by controlled-potential bulk electrolyses using equipment described in the cyclic voltammetry section. The cell used is described in ref 33. The reference electrode was an aqueous (saturated KCl) calomel electrode. Concentrations were approximately 1 mM with 0.1 M TBAP. After electrooxidation the sample was concentrated by evaporation under vacuum, transferred to a quartz EPR tube, and deaerated with nitrogen. Resulting sample concentrations were approximately 10 mM. A Varian E-Line Century Series spectrometer equipped with a Varian E102 X-band microwave bridge was used to obtain EPR spectra at a modulation frequency of 100 kHz. 2,2-Bis(4-*tert*-octylphenyl)-1-picrylhydrazyl (DPPH), with a *g* value of 2.0036, was used as the calibration standard.

A Burmese ruby (lower level of $Cr^{3+}$ than common rubies and less easily saturated) was used to scale intensities. The ruby (2.5 mg after grinding) was attached to the side of the EPR tube using the radical-free adhesive Formvar (Monsanto, St. Louis, MO). Spectra were taken in a finger Dewar, both at room temperature and at 77 K, at microwave powers where no saturation was observed. Typical powers at 77 K were 10 mW for the Ni(III) signals, 0.40 mW for the ruby signal, and 0.01 mW for the very easily saturated porphyrinic cation radical signals. Linear responses of the console settings for modulation amplitude and gain were verified. The quartz tube with the ruby chip was rotated in the cavity until a set of lines was observed from the ruby that did not interfere with either the broad Ni(III) signal ($g \sim 2.24$, line width ~ 160 G) or the narrow porphyrinic cation radical signal ($g \sim 2.00$, line width ~ 10 G). Spectra were obtained first at room temperature and then at liquid-nitrogen temperature while the identical sample position in the cavity was maintained. Spectral acquisition was repeated at room temperature at the end of the run to verify that no significant change in the intensity of the porphyrinic cation radical signal had occurred with time. The approximate relative intensities of the signals ($I$) were obtained by using the expression $I \propto Y'_{max}(\Delta H_{pp})^2$, where $Y'_{max}$ is half the peak-to-peak amplitude and $\Delta H_{pp}$ is the peak-to-peak width of the first derivative spectrum.[34]

**Resonance Raman Spectra.** Exciting radiation was supplied by Coherent Innova Series 200 $Kr^+$ (406.7 and 413.1 nm) and Leconix HeCd (441.5 nm) lasers. The scattered radiation was collected in 135° backscattering geometry, and dispersed by a Spex 1403 double monochromator, detected by a cooled Hamamatsu R928P photomultiplier tube, using a Spex DM102 photon counting system, under the control of a Spex (IBM PC/AT-compatible) computer. Spectra were plotted by using Galactic Industries Lab Calc software and a Hewlett-Packard Color Pro plotter.

**Cyclic Voltammograms.** Cyclic voltammograms (CV's) were obtained with a Princeton Applied Research Model 173 potentiostat, Model 179 digital coulometer, and Model 175 universal programmer and a Yokagawa 3025 A4 X-Y recorder. The CV cell contained a Pt-foil working electrode (3 × 10 mm), a platinum-wire counter electrode, and an aqueous (saturated KCl) calomel reference electrode separated from the bulk solution with a Luggin capillary. Sample concentrations were approximately 0.1 mM.

## Results

**Oxidative Electrochemistry of NiOEP and Nickel β-Oxoporphyrins.** Redox potentials for NiOEP, NiMP, NiDP-II, and NiTP-A in 0.1 M TBAP/methylene chloride solution are listed in Table I. Figure 2A shows the cyclic voltammograms (CV's) of these compounds in methylene chloride solution. The first oxidation processes are characteristic of diffusion-controlled, reversible, one-electron processes as evidenced by the equal anodic and cathodic currents and the 0.059-V peak separations. Scan rate studies (from 10 to 200 mV/s) reveal linear peak current dependence on (scan rate)$^{1/2}$, as is expected for reversible, diffusion-controlled processes. As seen in Table I, the first oxidation potentials of the nickel β-oxoporphyrins in methylene chloride are within 0.15 V of each other. The potentials are also similar to that of NiOEP. The second oxidation processes are reversible for the nickel tri-β-oxoporphyrins, but quasi-reversible for nickel mono-β-oxoporphyrin and the nickel di-β-oxoporphyrins. Peak-to-peak separations for the latter range from 0.13 to 0.26 V. The

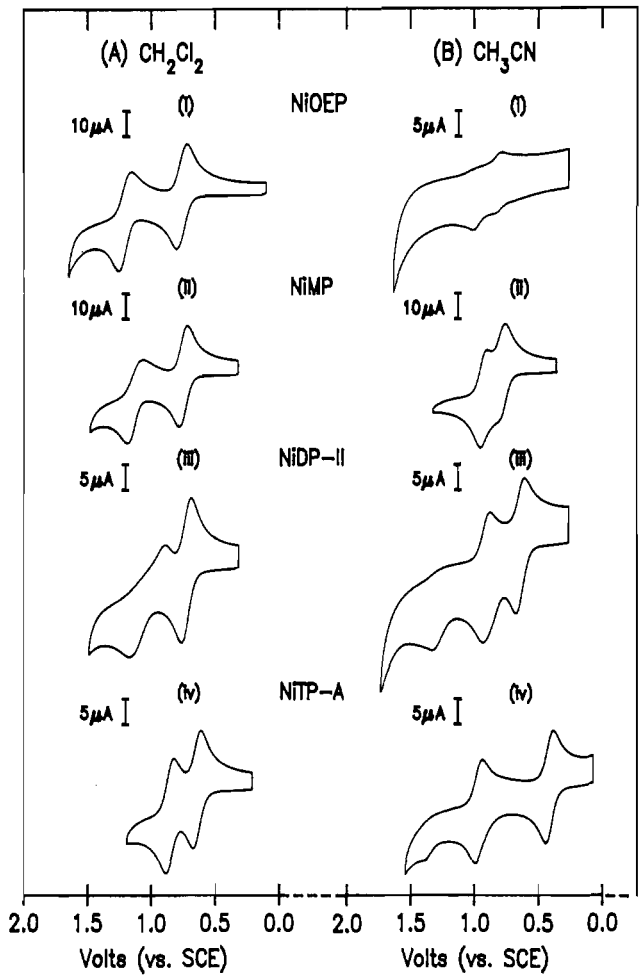


**Figure 2.** Cyclic voltammograms in 0.1 M TBAP/$CH_2Cl_2$ (A) and 0.1 M TBAP/$CH_3CN$ (B) of NiOEP (i), NiMP (ii), NiDP-II (iii), and NiTP-A (iv). Scan rate was 50 mV/s.

**Table I.** Redox Potentials ($E°$'s) (vs SCE) for NiOEP, NiOEC,[a] NiOEiBC,[a] and Nickel β-Oxoporphyrins[b]

| | acetonitrile | | | methylene chloride | | |
|---|---|---|---|---|---|---|
| compd | ox. 1 | ox. 2 | ox. 3 | ox. 1 | ox. 2 | ox. 3 |
| NiOEP | 0.75 | 0.94 | ... | 0.77 | 1.23 | ... |
| NiMP | 0.73 | 0.88 | ... | 0.74 | 1.13[d] | ... |
| NiDP-I | 0.55 | 0.87 | 1.2[c] | 0.69 | 1.03[d] | ... |
| NiDP-II | 0.58 | 0.84 | 1.2[c] | 0.71 | 1.01[d] | ... |
| NiDP-III | 0.64 | 0.92 | ... | 0.78 | 1.04[d] | ... |
| NiDP-IV | 0.59 | 0.87 | 1.2[c] | 0.71 | 1.03[d] | ... |
| NiDP-V | 0.58 | 0.83 | 1.2[c] | 0.69 | 1.01[d] | ... |
| NiTP-A | 0.34 | 0.90 | 1.3[c] | 0.63 | 0.85 | ... |
| NiTP-B | 0.36 | 0.86 | 1.3[c] | 0.66 | 0.83 | ... |
| NiOEC | 0.48 | 0.82 | | 0.48 | 1.03 | |
| NiOEiBC | 0.22 | 0.61 | | 0.21 | 0.86 | |

[a] From ref 21. [b] Porphyrin concentration was approximately 0.1 mM; electrolyte was 0.1 M tetrabutylammonium perchlorate. Scan rate was 50 mV/s. [c] Inequivalent anodic and cathodic peak heights. [d] $E_{pa} - E_{pc}$ greater than $0.059/n$ V.

(33) Czernuszewicz, R. S.; Macor, K. A. *J. Raman Spectrosc.* **1988**, *19*, 553–557.
(34) Wertz, J. E.; Bolton, J. R. In *Electron Spin Resonance: Elementary Theory and Practical Applications*; MacGraw Hill: New York, 1972; Chapter 2.

**Table II.** EPR Data for Oxidized NiOEP and Oxidized Nickel β-Oxoporphyrins in Methylene Chloride and Acetonitrile at 20 °C and Liquid-Nitrogen Temperature

| one-electron-oxidized compd | $g_{av}$ value (width, G) | | | |
|---|---|---|---|---|
| | methylene chloride | | acetonitrile | |
| | 20 °C | $N_2$(l) | 20 °C | $N_2$(l) |
| NiOEP | 2.003 (13) | 2.003 (12) | insufficient solubility | |
| NiMP | 2.003 (11) | 2.003 (11) | 2.003 (8) | 2.003 (12) |
| NiDP-II | 2.003 (12) | 2.003 (11) | no signal | 2.240 (160) |
| NiTP-A | no signal | 2.240 (160) | no signal | 2.235 (145) |

second oxidation potentials are approximately 0.2 V lower for the nickel tri-β-oxoporphyrins compared to the nickel di-β-oxoporphyrins.

Redox potentials for NiOEP, NiMP, NiDP-II, and NiTP-A in 0.1 M TBAP/acetonitrile solution are also listed in Table I. Figure 2B shows the cyclic voltammograms of these compounds in acetonitrile solution. The first and second oxidation processes are characteristic of diffusion-controlled, reversible, one-electron processes as evidenced by the equal anodic and cathodic currents and the 0.059-V peak separations. Scan rate studies (from 10 to 200 mV/s) reveal linear peak current dependence on (scan rate)$^{1/2}$, as is expected for reversible, diffusion-controlled processes. The second oxidation potentials are very similar for all of the nickel β-oxoporphyrins. An anodic peak (without a corresponding cathodic peak) is observed at potentials above the second oxidation in both the nickel di- and tri-β-oxoporphyrins.

The first oxidation potentials of NiOEP and NiMP are nearly identical in methylene chloride and acetonitrile. In contrast, the first oxidation potentials of the nickel di-β-oxoporphyrins differ by approximately 0.12 V in these two solvents. An even larger redox potential difference of 0.30 V is found between these solvents for the nickel tri-β-oxoporphyrins. To gauge the sensitivity of the porphyrin ring oxidation process to solvents, we compared the effect of acetonitrile and methylene chloride on the $P^{\bullet+}/P$ redox potential of the metal redox-inactive MgOEP. It is known that Zn and Mg porphyrins exhibit negative shifts in $P^{\bullet+}/P$ redox potential upon coordination of axial ligands.[35] We found the $MgOEP^{\bullet+}/MgOEP$ potentials to be 0.51 and 0.49 V in methylene chloride and acetonitrile, respectively, indicating that porphyrin ring oxidations are not significantly sensitive to differences between these two solvents.

The second oxidation potentials are significantly higher in methylene chloride than in acetonitrile for NiOEP and the mono- and di-β-oxoporphyrins. The differences are 0.29 (NiOEP), 0.25 (NiMP), and 0.16 V (average for nickel di-β-oxoporphyrins). In contrast, the tri-β-oxoporphyrin second oxidation potentials are nearly identical in these two solvents.

**EPR Characterization of the One-Electron-Oxidation Products of NiOEP and Nickel β-Oxoporphyrins.** EPR spectra of the products of the first oxidations of NiOEP, NiMP, NiDP-II, and NiTP-A were measured at both room temperature and liquid-nitrogen temperatures in methylene chloride and acetonitrile solutions. The data are presented in Table II. As expected, NiOEP is oxidized to a porphyrin cation radical with a $g$ value of 2.003 in methylene chloride at room temperature and liquid-nitrogen temperature. NiOEP is not sufficiently soluble in acetonitrile to obtain EPR spectra of its oxidation products in this solvent.

NiMP is oxidized to a β-oxoporphyrin cation radical with a $g$ value of 2.003 in both methylene chloride and acetonitrile. In acetonitrile, $E°$'s for the first and second oxidation processes differ by only 0.15 V. When the electrolysis potential is raised slightly above $E°$ of the first oxidation (0.73 V), the solution exhibits two distinct EPR signals at liquid-nitrogen temperature. One signal at $g = 2.003$ is identical in both width and $g$ value to the nickel β-oxoporphyrin cation radical signal seen in methylene chloride, while the other signal at $g_{av} = 2.243$ is very broad (160 G). The latter is similar to that observed from Ni(III) species, such as nickel(III) glycine complexes, which have a $g_{av}$ value in the range of 2.11–2.20,[36] and $Ni^{III}TPP$, which has a $g_{av}$ of 2.219.[20a] The $g_{av} = 2.243$ signal grows as the electrolysis potential approaches $E°$ of the second oxidation process, which strongly suggests that the second oxidation process yields a $Ni^{III}MP^{\bullet+}$ species.

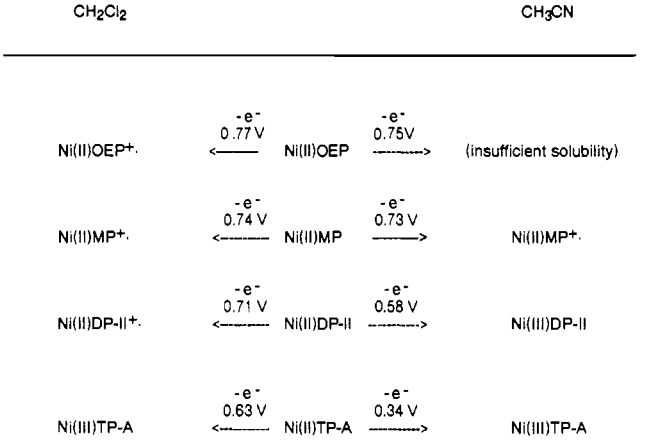


**Figure 3.** Scheme summarizing the effect of solvent on the identity of the one-electron-oxidation products of NiOEP, NiMP, NiDP-II, and NiTP-A.

The one-electron-oxidized NiDP-II species in methylene chloride at room temperature is a typical nickel(II) porphyrinic cation radical with a $g = 2.003$ signal. At liquid-nitrogen temperature as the electrolysis potential is raised toward $E°$ of the second oxidation process, a broad (160 G) $g_{av} = 2.236$ signal is observed in addition to the $g = 2.003$ signal. Presumably, the second oxidation process in methylene chloride generates a $Ni^{III}DP\text{-}II^{\bullet+}$ species, since the $g_{av} = 2.236$ signal grows as the electrolysis potential approaches $E°$ of the second oxidation. In acetonitrile at liquid-nitrogen temperature, a strong Ni(III) signal with $g_{av} = 2.240$ is seen. The Ni(III) signal is quasi-axial and does not exhibit hyperfine splitting. The Ni(III) signal is not observed at room temperature, presumably due to line broadening.

One-electron-oxidized NiTP-A exhibits a broad signal at $g_{av} = 2.240$ in methylene chloride at liquid-nitrogen temperature, indicating that the nickel tri-β-oxoporphyrin is oxidized to a $Ni^{III}TP\text{-}A$ species. No Ni(III) signal is observed at room temperature in this solvent. Similarly, at liquid-nitrogen temperature in acetonitrile, a strong signal is seen at $g_{av} = 2.235$ from $Ni^{III}TP\text{-}A$. As in methylene chloride, no Ni(III) signal is observed at room temperature in acetonitrile. Both Ni(III) signals are quasi-axial and do not exhibit hyperfine splitting.

The EPR results provide clear evidence for the production of the Ni(III) state at room temperature in NiDP-II and NiTP-A. These are the first unambiguous examples of nickel(III) porphyrinic compounds that are stable at room temperature. A solvent-induced switch in the site of one-electron abstraction occurs in NiDP-II, where a $Ni^{III}DP\text{-}II$ species is produced in acetonitrile solution and a $Ni^{II}DP\text{-}II$ cation radical is generated in methylene chloride solution. In both solvents, one-electron oxidation of NiMP yields a $Ni^{II}MP$ cation radical while one-electron oxidation of NiTP-A yields $Ni^{III}TP\text{-}A$ species. The scheme in Figure 3 summarizes the oxidation products observed in the two solvents.

**NMR Spectroscopy of NiMP, NiDP-II, and NiTP-B in Acetonitrile Solution.** In acetonitrile, NiMP exhibited small shifts (0.07–0.22 ppm) in the positions of the methine proton resonances relative to chloroform. Similar shifts (0.03–0.16 ppm) were observed for the methine protons of NiDP-II. NiTP-B exhibited drastically broadened peaks in this solvent, and its methine proton

(35) Fajer, J.; Borg, D. C.; Forman, A.; Felton, R. H.; Vegh, L.; Dolphin, D. *Ann. N.Y. Acad. Sci.* **1973**, *206*, 349–356.

(36) Margerum, D. W.; Anliker, S. L. In *The Bioinorganic Chemistry of Nickel*; Lancaster, J. R., Ed.; VCH Publishers: New York, 1988; Chapter 2.

(37) Scheer, H.; Inhoffen, H. H. In *The Porphyrins*; Dolphin, D., Ed.; Academic Press: New York, 1978; Vol. 2, Chapter 2.

**Table III.** Observed Raman Band Frequencies ($cm^{-1}$) and Polarizations for NiOEP,[a] NiOEC,[b] and Nickel β-Oxoporphyrins

| | mode | composition | NiOEP | NiOEC | NiMP | NiDP-I | NiDP-II | NiDP-III | NiDP-IV | NiDP-V |
|---|---|---|---|---|---|---|---|---|---|---|
| $A_1$ | | $\nu$(C=O) | | | 1711 p | 1708 p | 1716 p | 1714 p | 1708 p | 1710 p |
| $B_{1g}$ | $\nu_{10}$ | $\nu(C_\alpha C_m)_{asym}$ | 1653 dp | 1648 p | 1656 dp | 1649 ap | 1653 dp | 1655 ap | 1653 dp | 1650 ap |
| $E_u$ | $\nu_{37a}$ | $\nu(C_\alpha C_m)_{asym}$ | 1637 calc | 1614 p | 1609 p | 1609 p | 1611 p | 1616 p | 1591 p | 1582 p |
| $E_u$ | $\nu_{37b}$ | $\nu(C_\alpha C_m)_{asym}$ | 1637 calc | 1608 | 1591 dp | 1609 dp | 1611 dp | | 1594 dp | |
| $A_{1g}$ | $\nu_2$ | $\nu(C_\beta C_\beta)$ | 1600 p | 1588 p | | | 1567 p | | 1572 p | |
| $A_{2g}$ | $\nu_{19}$ | $\nu(C_\alpha C_m)_{asym}$ | 1603 ap | 1590 ap | | 1575 ap | 1586 ap | | | 1580 ap |
| $B_{1g}$ | $\nu_{11}$ | $\nu(C_\beta C_\beta)$ | 1575 dp | 1546 p | 1564 dp | | 1557 dp | 1566 dp | | |
| $A_{1g}$ | $\nu_3$ | $\nu(C_\alpha C_m)_{sym}$ | 1519 p | 1512 p | 1523 p | 1533 p | 1522 p | 1505 p | 1529 p | 1532 p |
| $B_{2g}$ | $\nu_{28}$ | $\nu(C_\alpha C_m)_{sym}$ | 1483 dp | 1478 dp | 1486 p | 1484 p | 1497 p | | 1477 p | 1484 p |
| $E_u$ | $\nu_{40a}$ | $\nu$(pyr $^1/_4$ ring) | 1396 | 1382 p | 1383 p | 1385 p | 1387 p | 1382 p | 1393 p | |
| $E_u$ | $\nu_{40b}$ | $\nu$(pyr $^1/_4$ ring) | 1396 | | 1404 dp | 1385 dp | | | | 1385 dp |
| $B_{2g}$ | $\nu_{29}$ | $\nu$(pyr $^1/_4$ ring) | 1408 dp | 1402 dp | | 1406 p | 1403 p | | | |
| $A_{1g}$ | $\nu_4$ | $\nu$(pyr $^1/_2$ ring)$_{sym}$ | 1383 p | 1367 p | 1356 p | | 1355 p | 1361 p | 1366 p | 1360 p |
| $E_u$ | $\nu_{41a}$ | $\nu$(pyr $^1/_2$ ring)$_{sym}$ | 1346 calc | 1349 p | 1346 p | 1345 p | 1341 p | 1340 p | 1343 p | |
| $E_u$ | $\nu_{41b}$ | $\nu$(pyr $^1/_2$ ring)$_{sym}$ | 1346 calc | | | 1345 dp | | | | 1346 dp |
| $A_{2g}$ | $\nu_{21}$ | $\delta$(C$_m$H) | 1309 ap | 1308 ap | 1307 ap | 1310 dp | | 1303 dp | 1304 ap | 1306 ap |
| $E_u$ | $\nu_{42a}$ | $\delta$(C$_m$H) | 1231 | | 1234 p | 1230 p | | 1232 p | 1236 p | |
| $E_u$ | $\nu_{42b}$ | $\delta$(C$_m$H) | 1231 | | | 1236 dp | 1247 dp | | | 1233 ap |
| $B_{1g}$ | $\nu_{13}$ | $\delta$(C$_m$H) | 1220 dp | 1232 p | 1212 dp | 1207 ap | | 1202 ap | | |
| $E_u$ | $\nu_{43a,b}$ | $\nu$(pyr $^1/_2$ ring) | 1153 | | 1156 dp | 1155 p/dp | 1166 p/dp | 1154 dp | 1148 dp | 1152 dp |
| $E_u$ | $\nu_{44a,b}$ | $\nu(C_\beta C_1)$ | 1133 | | 1133 p/dp | 1141 dp | 1131 p/dp | 1138 dp | 1139 dp | 1132 p/dp |
| $A_{1g}$ | $\nu_5$ | $\nu(C_\beta C_1)_{sym}$ | 1139 p | 1146 p | 1220 p | 1227 p | 1228 p | | 1221 p | |
| $A_{2g}$ | $\nu_{22}$ | $\nu$(pyr $^1/_2$ ring) | 1121 ap | 1124 ap | 1121 dp | 1119 ap | 1117 dp | 1115 ap | | |
| $E_u$ | $\nu_{46a}$ | $\delta$(pyr def)$_{asym}$ | 927 | 926 p | 922 p | | 919 p | 930 p | 927 p | 924 p |
| $A_{1g}$ | $\nu_6$ | $\nu$(pyr breath) | 804 p | 798 p | | 802 p | 801 p | 801 p | 801 p | 801 p |
| E | | $CH_2$ wag | 1378 calc | 1375 calc | 1371 p | 1371 p | | | 1362 p | |
| $A_1$ | | $CH_2$ wag | 1316 p | 1328 | 1316 p | | 1314 p | | 1317 p | |
| $A_1$ | | $CH_2$ twist | 1260 p | 1274 | 1263 p | 1264 p | | 1271 p | 1269 p | 1263 p |
| $B_1$ | | $CH_2$ twist | 1276 dp | 1261 | 1272 dp | 1275 dp | 1269 dp | 1258 dp | | |
| $A_1$ | | $\nu(C_1C_2)$ | 1025 p | 1020 p | | | | | 1011 p | 1012 p |
| $B_1$ | | $\nu(C_1C_2)$ | 1024 dp | 1062 | 1020 dp | 1022 dp | 1023 dp | | | 1024 dp |
| $B_2$ | | $\nu(C_1C_2)$ | 1023 calc | 961 dp | 958 ap | 961 dp | 965 dp | | 958 p | 958 dp |

[a] Assignments and certain frequencies from ref 24. [b] Assignments and frequencies from ref 25a. Key: p = polarized, dp = depolarized, ap = anomalously polarized, and calc = calculated and not observed.

resonances were not identifiable.

**Resonance Raman Spectroscopy of Nickel β-Oxoporphyrins.** Raman band assignments for the β-oxoporphyrins were made using the established assignments for NiOEP,[24] NiOEC,[25] and NiOEiBC[26] as references. The assignments are naturally tentative because we have not carried out studies with isotopically labeled β-oxoporphyrins. Table III lists the observed Raman band frequencies along with their polarization properties and assignments.

Table III reveals that all of the nickel β-oxoporphyrins examined show a band near 1710 $cm^{-1}$, which is absent in the resonance Raman (RR) spectrum of NiOEP. This mode has been assigned to $\nu$(C=O).[27,28] The band occurs within the fairly narrow frequency range 1708–1716 $cm^{-1}$. The small frequency differences probably result from slightly varying amounts of carbonyl–pyrrole ring conjugation. Heme $d_1$ from dissimilatory nitrite reductase contains isomer DP-II.[8] This isomer has the highest frequency for $\nu$(C=O), indicating that it has the most highly reduced pyrrole rings of the di-β-oxoporphyrins. The carbonyl stretching mode at 1716 $cm^{-1}$ exhibits the greatest relative enhancement in the 406.7-nm-excited spectrum of NiDP-II (Figure 4a) where it is the strongest band in the spectrum, whereas in the 441.5-nm spectrum (Figure 4b) it has moderate intensity. A Raman band at 1715 $cm^{-1}$ has been observed from reduced nitrite reductase heme $cd_1$ with 457.9-nm excitation.[28] Our results indicate that the best enhancement of the carbonyl stretch in heme $d_1$ is expected with violet excitation.

The electronic absorption spectra of the β-oxoporphyrins resemble chlorins more than porphyrins. Split Soret bands and strong red absorptions are observed in both chlorin[37] and β-oxoporphyrin spectra (inset Figure 5c). The position of the red band in the β-oxoporphyrins is highly variable within the five isomeric di-β-oxoporphyrins, ranging from 621 nm in NiDP-II to 706 nm in NiDP-V. The Soret band pattern is also distinctive for each di-β-oxoporphyrin. NiDP-I (inset Figure 5c), NiDP-II (inset Figure 4), NiDP-III, and NiDP-V each have two bands in this region, while NiDP-IV (inset Figure 6) has three bands. Clearly the pattern of β-oxo group substitution has a significant effect on the electronic absorption spectrum.

Examination of the RR spectra in Figure 5 of NiOEP, NiMP, and NiDP-I reveals significant differences. In the Soret-excited spectra of porphyrins, the strongest bands are porphyrin ring stretching modes $\nu_4$, $\nu_3$, and $\nu_2$. In NiOEP (Figure 5a) these are seen at 1383, 1519, and 1600 $cm^{-1}$, respectively. $\nu$(C=O), $\nu_{37a}$, $\nu_{11}$, $\nu_3$, and $\nu_{40a}$ are the strongest bands in the spectrum of NiMP (Figure 5b) and are seen at 1711, 1609, 1564, 1523, and 1383 $cm^{-1}$, respectively. In the spectrum of NiDP-I (Figure 5c), $\nu$(C=O), $\nu_{19}$, $\nu_3$, and $\nu_{40b}$ are the most intense bands and are observed at 1708, 1575, 1533, and 1385 $cm^{-1}$, respectively. Modes $\nu_2$ and $\nu_4$ have not been identified in NiDP-I. These two bands have been observed in other di-β-oxoporphyrins (Table III), but are not usually among the strongest bands in a typical spectrum.

A large number of $E_u$ modes are strongly enhanced in the β-oxoporphyrin spectra. Raman-inactive $E_u$ modes can become Raman-active A and B modes as the effective molecular symmetry becomes lower than $D_{4h}$. In the NiDP-I spectrum (Figure 5c), $\nu_{40b}$ is observed at 1385 $cm^{-1}$ and is one of the strongest bands. Mode $\nu_{41b}$ at 1345 $cm^{-1}$ also has appreciable intensity. Modes $\nu_{37a}$ at 1609 $cm^{-1}$ and $\nu_{40a}$ at 1383 $cm^{-1}$ are strongly enhanced in the spectrum of NiMP (Figure 5b). It is interesting that $E_u$ modes $\nu_{37a}$ and $\nu_{37b}$ seen at 1611 $cm^{-1}$ in the spectra of NiDP-II are enhanced with different excitation wavelengths within the Soret region. The depolarized nontotally symmetric mode ($\nu_{37b}$) is enhanced with 406.7-nm excitation (Figure 4a), and the polarized, totally symmetric component ($\nu_{37a}$) is observed with 441.5-nm excitation (Figure 4b). The 441.5-nm excitation is matched to the low-energy Soret peak while 406.7-nm excitation is within the high-energy Soret peak. NiDP-IV also exhibits this pattern. The depolarized mode ($\nu_{37b}$) is observed at 1594 $cm^{-1}$ with 406.7-nm excitation (Figure 6a), while the polarized component ($\nu_{37a}$) is seen at 1591 $cm^{-1}$ with 441.5-nm excitation (Figure 6c).

The pattern of β-oxoporphyrin mode enhancement varies with excitation wavelength. NiDP-IV provides a convenient example for study of the excitation pattern within the Soret band region. Figure 6 shows the spectra of NiDP-IV with 406.7-, 413.1-, and

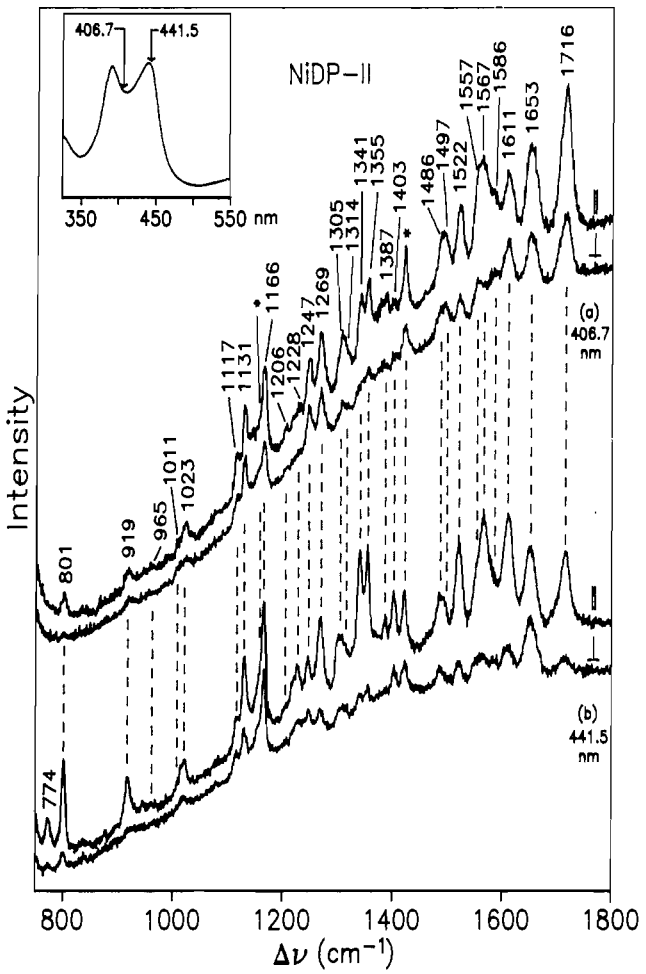


**Figure 4.** Resonance Raman spectra in parallel and perpendicular polarizations for NiDP-II with 406.7- (a) and 441.5-nm (b) excitations. Conditions: (a) 100-mW laser power, 10-$cm^{-1}$ slit widths; (b) 20-mW laser power, 8 $cm^{-1}$ slit widths. Asterisks indicate $CH_2Cl_2$ solvent bands. The inset shows the electronic absorption spectrum of NiDP-II marked with laser excitation wavelengths.

441.5-nm excitation wavelengths. As can be seen in the absorption spectrum (inset), 413.1 and 441.5 nm are approximately matched to the second and third absorption maxima, while 406.7 nm is on the side of the second maximum. Modes $\nu_4$ and $\nu_2$ at 1366 and 1572 $cm^{-1}$, respectively, are two of the strongest bands in the 406.7-nm-excited spectrum. These bands are considerably weaker in the 413.1-nm spectrum and are not observed at all with 441.5-nm excitation. In contrast to NiDP-IV, modes $\nu_4$ and $\nu_2$ at 1355 and 1567 $cm^{-1}$, respectively, retain appreciable intensity in NiDP-II.

## Discussion

**EPR and Electrochemical Characterization of Nickel β-Oxoporphyrins.** As is seen in Table I, redox potentials for the first oxidation process in acetonitrile decrease as follows: 0.75 (NiOEP), 0.73 (NiMP), 0.58 (NiDP-II), and 0.34 V (NiTP-A). At first glance, this trend appears in keeping with the fact that chlorins and isobacteriochlorins are more easily oxidized than porphyrins.[22] For example, the potentials for the nickel octaethyl derivatives are 0.48 (NiOEC) and 0.22 V (NiOEiBC).[22] However, a problem with this rationale is that in methylene chloride solution the first oxidation half-wave potentials exhibit a considerably smaller range (Table I): 0.77 (NiOEP), 0.74 (NiMP), 0.71 (NiDP-II), and 0.63 V (NiTP-A).

Stolzenberg has reported potentials in acetonitrile for the oxidations and reductions of the free-base mono-β-oxoporphyrin and several di-β-oxoporphyrins as well as the copper, manganese, zinc, and nickel mono-β-oxoporphyrins.[18] As in the present work, the potentials for metallo-MP oxidations were found to be quite similar to those for their MOEP analogues.

The EPR spectral data of the one-electron-oxidation products of NiDP-II (Table II) show that a solvent-induced switch in the site of the first electron abstraction occurs, where a $Ni^{III}$DP-II series is produced in acetonitrile solution and a $Ni^{II}$DP-II cation radical is generated in methylene chloride solution. The EPR results (Table II) demonstrate that in both acetonitrile and methylene chloride solvents one-electron oxidation of NiMP yields a $Ni^{II}$MP cation radical while one-electron oxidation of NiTP-A yields $Ni^{III}$TP-A species. The scheme in Figure 3 summarizes the oxidation products observed in the two solvents.

The second oxidation potentials are significantly higher in methylene chloride than in acetonitrile for NiOEP and the mono- and di-β-oxoporphyrins. The differences are 0.29 (NiOEP), 0.25 (NiMP), and 0.16 V (average for Ni dioxoporphyrins). The large difference in potentials probably indicates different types of redox processes in the two solvents. We postulate that for NiOEP and NiMP in acetonitrile the second electron is probably removed from the Ni(II) center to generate the nickel(III) porphyrin cation radical. A Ni(III) EPR signal ($g_{av}$ = 2.243) was observed from NiMP when the electrolysis potential approached $E°$ of the second oxidation. In methylene chloride, where there should be no special stabilization of the Ni(III) state, the second electron probably comes from the porphyrin ring and yields the porphyrin dication.

For the nickel di-β-oxoporphyrins in acetonitrile, since the first electron is removed from the Ni(II) center, the second electron is lost from the porphyrin ring to yield a nickel(III) porphyrin cation radical. For the nickel di-β-oxoporphyrins in methylene chloride, the second electron is likely lost from the Ni center, since a Ni(III) signal ($g_{av}$ = 2.236) was observed when the electrolysis potential approached $E°$ of the second oxidation. The nickel tri-β-oxoporphyrins appear to behave like the nickel di-β-oxoporphyrins in acetonitrile with the first and second electrons coming from the Ni(II) center and the porphyrinic ring, respectively. In methylene chloride since the first electron is removed from the NiTP metal center, the second electron oxidation product must be the nickel(III) tri-β-oxoporphyrin cation radical.

It is clear from the data in Figure 3 that within the octaethyl series Ni(III) is stabilized by increasing numbers of β-oxo groups and a coordinating solvent. It is important to understand how these factors lead to the stabilization of Ni(III) in these complexes. In particular, it is of interest to understand why the di- and tri-β-oxoporphyrin rings stabilize Ni(III) to such a great extent while porphyrin, mono-β-oxoporphyrin, chlorin, and isobacteriochlorin rings do not.

**Axial Ligation.** One-electron oxidation of NiDP's generates nickel(II) di-β-oxoporphyrin cation radicals in methylene chloride solution and nickel(III) di-β-oxoporphyrins in acetonitrile solution. It is reasonable to assume that acetonitrile acts as a ligand to form either five- or six-coordinate complexes. The solvent-dependent switch in the character of the HOMO from di-β-oxoporphyrin-centered to nickel-centered and the corresponding increase in HOMO energy, which is reflected in the 0.15-V lower first oxidation redox potential can, in fact, be explained by axial ligation.

Figure 7 illustrates the molecular orbital energy levels for a four-coordinate square-planar porphyrin and a six-coordinate tetragonally distorted porphyrin. In the four-coordinate species, the HOMO is a β-oxoporphyrin $\pi$ orbital. The four-coordinate porphyrin is typically low-spin due to the large energy difference between the $d_{xy}$ and the $d_{x^2-y^2}$ porphyrin $\sigma^*$ orbitals. Interaction of the nickel $d_{z^2}$ orbital with the acetonitrile $p_z$ orbitals forms either three (six-coordinate) or two (five-coordinate) molecular orbitals. The result is that in the axially ligated species the HOMO is the antibonding Ni-centered $p_z - d_{z^2} + p_z$ orbital. The higher energy of this orbital in the six-coordinate species compared to the β-oxoporphyrin $\pi$ HOMO in the four-coordinate complex is reflected both in the lower first oxidation potential of the former in acetonitrile and in the fact that the first electron is removed from the Ni(II) center in acetonitrile. The six-coordinate porphyrin can be either high or low spin since the energy difference between the axial ligand $p_z - d_{z^2} + p_z$ orbital and the $d_{x^2-y^2}$ porphyrin $\sigma^*$ orbital is small. A five-coordinate porphyrin would have the same

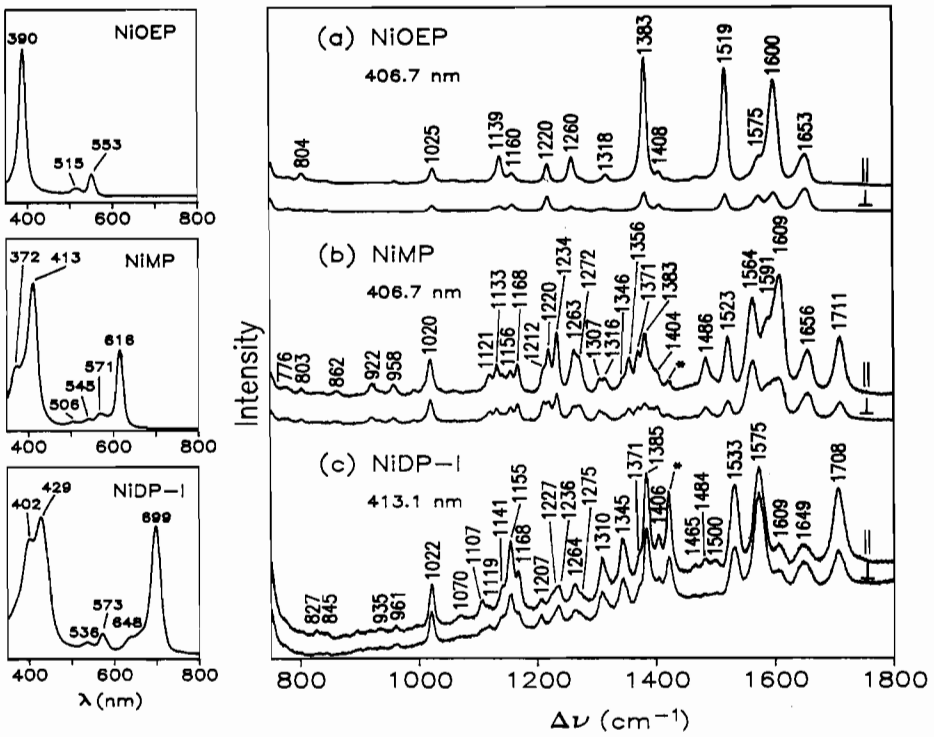


**Figure 5.** Resonance Raman and electronic absorption spectra of NiOEP (a), NiMP (b), and NiDP-I (c). RR spectra were obtained in parallel and perpendicular polarizations under the following conditions: (a) 406.7-nm excitation, 100-mW laser power, 10-$cm^{-1}$ slit widths; (b) 406.7-nm excitation, 70-mW laser power, 10-$cm^{-1}$ slit widths; (c) 413.1-nm excitation, 70-mW laser power, 10-$cm^{-1}$ slit widths. Asterisks indicate $CH_2Cl_2$ solvent bands.

relative orbital ordering as the six-coordinate case, but the destabilization of the $d_{z^2}$ orbital would be approximately half as large.

One-electron oxidation of nickel tri-β-oxoporphyrins yields nickel(III) tri-β-oxoporphyrins in both methylene chloride and acetonitrile solutions. In the case of methylene chloride solutions, the electrolytic anion, perchlorate, could function as an axial ligand. Perchlorate-stabilized $Ni^{III}TPP$ (TPP = *meso*-tetraphenylporphyrin) has been reported.[20] When methylene chloride or benzonitrile solutions of $Ni^{II}TPP^{\bullet+}$ were cooled to liquid-nitrogen temperature, an EPR signal characteristic of $Ni^{III}TPP$ was observed. Perchlorate or hexafluorophosphate anions were required to observe Ni(III). Interestingly, other nickel *meso*-tetraaryl- and -tetraalkylporphyrins do not form Ni(III) species.[38] It is also possible that intermolecular axial ligation of β-oxo groups stabilizes Ni(III) in methylene chloride solution.[39]

**Ring Ruffling and Axial Ligation.** It is known from crystallographic data on *free-base* rings that the hole size increases with increasing saturation of the ring.[10b,39] The result of this trend for *nickel* complexes is that the extent of ring ruffling, as measured by the methine carbon deviation from the plane of the four nitrogens, increases with increasing ring saturation. The more reduced the ring, the more "flexible" it is (since it has lower π-conjugation) and the more it can contract to bind the Ni(II) ion with a bond length that leads to a stable Ni(II) complex.

Figure 8 illustrates the ruffling patterns that have been observed in the crystal structures of NiMP,[18] NiDP-II,[23] NiTP-A,[23] nickel *meso*-tetramethylchlorin (NiTMC),[41] and nickel *meso*-tetramethylisobacteriochlorin (NiTMiBC).[42] The radii of the circles are proportional to the deviation from the mean plane defined by the four nitrogens. A term $d_m$ has been used to denote this (average) number for the methine carbons, and the $d_m$ values are listed in parentheses in the caption to Figure 8 after each name.

The tendency toward axial ligation in Ni(II) has been shown to directly correlate with the extent of ring ruffling.[10b] Eschenmoser has reported the following series of increasing axial ligation tendency:[10b] corrin < porphyrin < chlorin < isobacteriochlorin < bacteriochlorin < pyrrocorphin. On the basis of our recently determined $d_m$ values, we have inserted the β-oxoporphyrins into Eschenmoser's series: corrin < porphyrin < mono-β-oxoporphyrin < di-β-oxoporphyrin < tri-β-oxoporphyrin < chlorin < isobacteriochlorin < bacteriochlorin < pyrrocorphin.

From the tri-β-oxoporphyrin position upward to pyrrocorphin, the complexes appear to bind axial ligands so strongly that they become high spin. (A high-spin nickel chlorin complex has not yet been reported.) Stronger axial ligation would lead to a smaller energy gap between the $p_z - d_{z^2} + p_z$ and the $d_{x^2-y^2}$ porphyrin $\sigma^*$ orbitals (Figure 7). The evidence that is suggestive of high-spin complexes is significant NMR peak broadening in coordinating solvents. We have found that the NMR spectrum of $Ni^{II}TP$-B shows significant peak broadening in acetonitrile solution, whereas sharp signals are observed in chloroform. Similar NMR spectral broadening has been reported for nickel(II) octaethylpyrrocorphinates in acetonitrile and methanol, but not in methylene chloride,[10b] and for nickel(II) octaethylbacteriochlorin and nickel(II) octaethylisobacteriochlorin in methanol, but not in acetonitrile.[10b] In order to obtain unambiguous evidence for paramagnetism, Evans' method magnetic susceptibility measurements would be necessary. We have found that NiMP and NiDP-II are diamagnetic in acetonitrile as well as chloroform, although there are significant NMR spectral shifts in acetonitrile solution.

The 0.30-V lower $Ni^{3+/2+}$ potential for NiTP's in acetonitrile compared to methylene chloride can be explained by stronger binding of acetonitrile versus perchlorate ligands. The energy of the HOMO $p_z - d_{z^2} + p_z$ orbital would be raised due to the strong acetonitrile ligand binding if the acetonitrile complex is low spin, or if the acetonitrile complex is high spin, the first electron would be removed from the high-energy $d_{x^2-y^2}$ porphyrin $\sigma^*$ orbital (Figure 7). In either case the electron would be removed from a Ni-centered orbital, and the redox potential would be lower in acetonitrile than in methylene chloride.

(38) (a) Kadish, K. M.; Sazou, D.; Liu, Y. M.; Saoiabi, A.; Ferhat, M.; Guilard, R. *Inorg. Chem.* **1988**, *27*, 1198–1204. (b) Chang, D.; Malinski, T.; Ulman, A.; Kadish, K. M. *Inorg. Chem.* **1984**, *23*, 817–824.
(39) Stolzenberg, A. M. *Inorg. Chim. Acta* **1987**, *138*, 1–4.
(40) Hoard, J. L. *Ann. N.Y. Acad. Sci.* **1973**, *206*, 18–31.
(41) Gallucci, J. C.; Swepston, P. N.; Ibers, J. A. *Acta Crystallogr.* **1982**, *B38*, 2134–2139.
(42) Suh, M. P.; Swepston, P. N.; Ibers, J. A. *J. Am. Chem. Soc.* **1984**, *106*, 5164–5171.

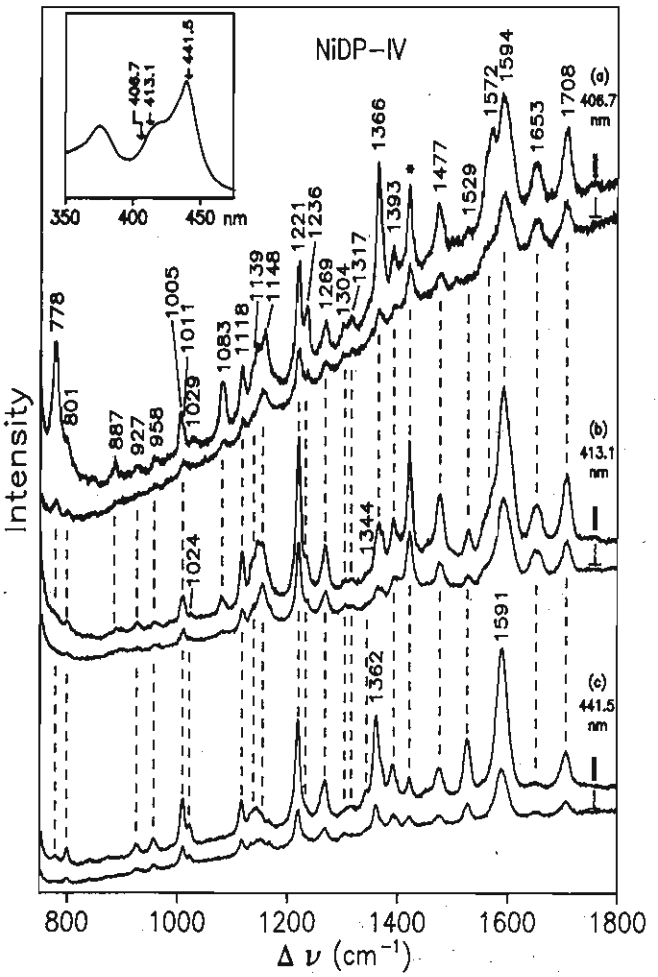


**Figure 6.** Resonance Raman spectra in parallel and perpendicular polarizations for NiDP-IV with 406.7- (a), 413.1- (b), and 441.5-nm (c) excitations. Conditions: (a) 100-mW laser power, 10-$cm^{-1}$ slit widths; (b) 70-mW laser power, 8-$cm^{-1}$ slit widths; (c) 20-mW laser power, 8-$cm^{-1}$ slit widths (c). Asterisks indicate $CH_2Cl_2$ solvent bands. Inset is the electronic absorption spectrum of NiDP-IV marked with laser excitation wavelengths.

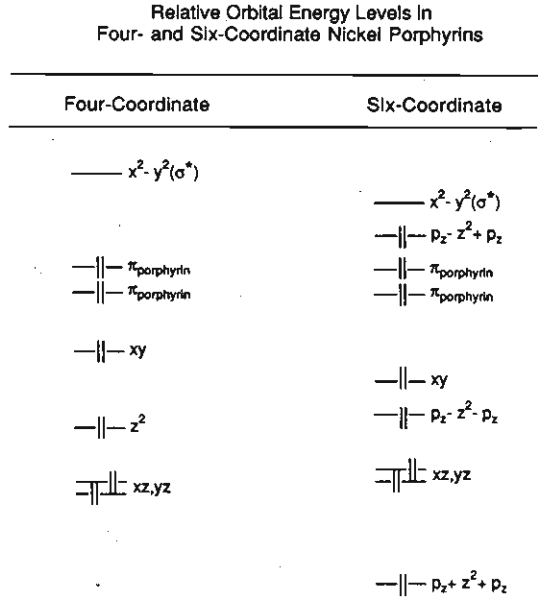


**Figure 7.** Molecular orbital scheme illustrating the relative orbital energy levels in four- and six-coordinate nickel(II) porphyrins.

**Stabilization of Ni(III): Correlation with Ring Ruffling and Axial Ligation.** The relative oxidation potentials for production of porphyrin cation radicals provide a measure of the relative

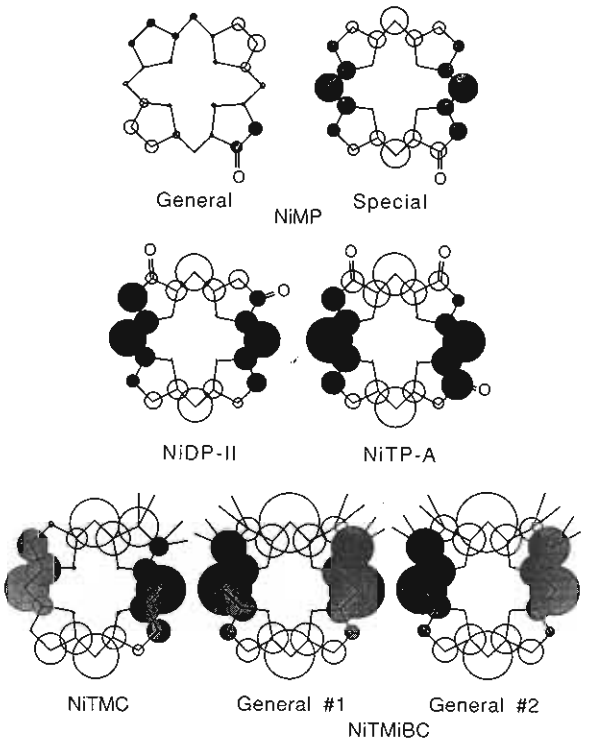


**Figure 8.** Illustration of the magnitude and symmetry of ruffling in NiMP (0.05, 0.35 Å)[18], NiDP-II (0.45 Å)[23], NiTP-A (0.51 Å),[23] NiTMC (0.58 Å)[41] and NiTMiBC (0.68, 0.65 Å).[42] The numbers in parentheses are $d_m$ values, which are methine carbon displacements from the plane defined by the four nitrogens. The radii of the circles are proportional to the displacement of the atoms from the plane defined by the four nitrogens. Shades of the circles indicate displacement either into or out of the plane of the paper.

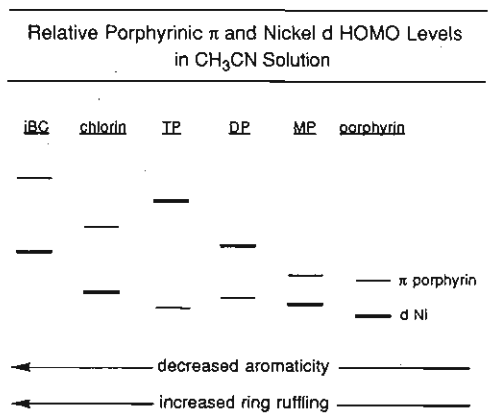


**Figure 9.** Illustration of the relative porphyrinic $\pi$ and nickel d HOMO levels in acetonitrile solution. (The lower levels shown are minimum values (with the lower level having an energy range between the upper and lower levels), since the second redox potential includes an additional energy required to remove an electron from an already oxidized species.) From right to left across the porphyrinic series aromaticity decreases and ring ruffling increases. Bold lines are Ni d HOMO's and fine lines are porphyrinic $\pi$ HOMO's. The high level of the Ni d HOMO's in DP and TP indicate stabilization of Ni(III) relative to the other porphyrinic ligands.

energies of the porphyrinic HOMO's. Table I lists the oxidation potentials for NiOEP, NiOEC, NiOEiBC, NiMP, the five isomeric nickel di-$\beta$-oxoporphyrins, and two isomeric nickel $\beta$-trioxoporphyrins in both acetonitrile and methylene chloride solvents.

The relative energy levels of the porphyrinic ligand $\pi$ orbital and the Ni $d_{xy}$ (for four-coordination) or $p_z - d_{z^2} + p_z$ (for six-coordination) orbitals are known from EPR experiments. In acetonitrile solution, we have shown that a Ni-centered orbital is the HOMO in NiDP and NiTP, whereas a porphyrinic $\pi$ orbital is the HOMO in NiMP. EPR results of Stolzenberg and Stershic

have demonstrated that in the same solvent a porphyrinic π orbital is the HOMO in NiOEP, NiOEC, and NiOEiBC.[21]

Figure 9 illustrates the relative energy levels of the highest occupied Ni d and porphyrinic π orbitals. The lower levels shown are minimum values (with the lower level having an energy range between the upper and lower levels), since the second redox potential includes an additional energy required to remove an electron from an already oxidized species. As one moves from right to left across the figure the aromaticity of the porphyrinic ligand decreases. Decreasing π-conjugation leads to larger intrinsic hole sizes.[10b,40] Proceeding from right to left across the series, progressively larger amounts of ring ruffling are required to contract the rings to a size which facilitates binding the small Ni(II) ion. This is the same direction in which the tendency for axial ligation increases as shown by Eschenmoser.[10b] Axial ligation can alleviate the strain of ruffling by donating electron density into the metal center and allowing the metal–nitrogen (porphyrinic) bonds to lengthen. In the extreme case of high-spin complex formation a planar structure can result since the Ni(II) ion is now considerably larger due to occupancy of the $d_{x^2-y^2}$ porphyrin $\sigma^*$ orbital. At some level of aromaticity axial ligation becomes sufficiently strong that the $p_z - d_{z^2} + p_z$ orbital rises above the porphyrinic π orbital. This crossover point occurs at the di-β-oxoporphyrin structure.

As one moves on to chlorin and isobacteriochlorin in Figure 9, the aromaticity has decreased to such a large extent that the porphyrinic π orbital is at a very high energy, and the first oxidation inevitably yields an organic radical. It has been suggested that the second oxidation of $Ni^{II}$OEiBC yields a Ni(III) organic radical.[21] The $Ni^{3+/2+}$ potential of NiOEiBC$^{\bullet+}$ (0.80 V)[21] is higher than that of the nickel di- and tri-β-oxooctaethylporphyrins because the electron is removed from a positively-charged species in the former case.

It is interesting to consider that the effect of adding a β-oxo group to the porphyrin ring is to cause a segmental decrease in the aromaticity of the porphyrin ring. Concomitant with this decrease in π-conjugation is a segmental increase in ring ruffling and presumably an increased tendency to bind axial ligands. The increased tendency to bind axial ligands results in lower $Ni^{3+/2+}$ potentials. It is clear that the β-oxoporphyrins are distinct compounds with properties bridging those of porphyrins and chlorins. Their particular balance of π-conjugation, ring ruffling, and axial ligation facilitates at least one example of metal redox chemistry that is inaccessible to other classes of octaethylporphyrinic ligands.

**Resonance Raman Spectroscopy.** Both chlorin and isobacteriochlorin have $C_2$ symmetry, but they have different two-fold symmetry axes. The symmetry axis passes through the reduced pyrrole ring in chlorin but between the two reduced rings in isobacteriochlorin. $B_{1g}$ and $B_{2g}$ modes correlate with A and B modes in chlorin, but with B and A modes in isobacteriochlorin. The $B_{1g}$ modes (now A) will be polarized in chlorin, while the $B_{2g}$ (now A) will be polarized in isobacteriochlorin. From Table III, it can be seen that $B_{1g}$ mode $\nu_{10}$ is depolarized ($\rho \sim 0.75$) in NiMP, NiDP-II, and NiDP-IV, whereas it is anomalously polarized ($\rho > 1$) in NiDP-I, NiDP-III, and NiDP-V. Mode $\nu_{10}$ is depolarized, anomalously polarized, and polarized in NiOEP,[24] NiOEiBC,[26] and NiOEC,[25a] respectively. $B_{2g}$ mode $\nu_{28}$ is polarized in all of the β-oxoporphyrins and NiOEiBC, whereas it is depolarized in both NiOEP and NiOEC. The depolarization ratios of bands $\nu_{10}$ and $\nu_{28}$ allow us to group all of the β-oxoporphyrins into the same effective symmetry class as NiOEiBC, $C_2''$. This classification is in contrast to NiOEC and NiOEP, which have effective $C_2'$ and $D_{4h}$ symmetries, respectively.

$A_{2g}$ (anomalously polarized) modes correlate with B modes in both chlorins and isobacteriochlorins. In chlorin, $A_{2g}$ modes can mix with $B_{2g}$ modes (both have B symmetry), while in isobacteriochlorin mixing can occur between $A_{2g}$ and $B_{1g}$ modes (both have B symmetry). In NiDP-I, NiDP-III, and NiDP-V mode $\nu_{10}$ is anomalously polarized, while in NiMP, NiDP-II, and NiDP-IV it is depolarized. The former three oxoporphyrins apparently have greater mixing between the anomalously polarized $A_{2g}$ (now B) mode $\nu_{19}$ and the depolarized $B_{1g}$ (now B) mode $\nu_{10}$, which increases the depolarization ratio of the latter. The fact that the polarization properties change but the $\nu_{10}$ frequencies remain near 1650 $cm^{-1}$ means that chlorins, isobacteriochlorins, porphyrins, and β-oxoporphyrins have similar mode compositions.

Close correspondence between NiOEP, NiOEC, and NiOEiBC vibrations has, in fact, been found from normal mode analyses of the three classes.[24,25a,26] The major spectral difference between porphyrins and the reduced rings, chlorins,[25,43] isobacteriochlorins,[26,44] and β-oxoporphyrins,[27] is the complicated pattern in the 1300–1400-$cm^{-1}$ region. $E_u$ modes that are activated by symmetry lowering are observed here with moderate to strong intensities.

RR spectral data for NiTP-A and NiTP-B have not been included in Table III, since the spectra are weak and complicated by fluorescence backgrounds. Several points deserve mention concerning the spectrum of NiTP-B, however. Two partially overlapping ν(C=O) bands are observed centered at 1708 $cm^{-1}$, and modes $\nu_{10}$ and $\nu_{11}$ are seen at 1644 and 1563 $cm^{-1}$, respectively, and are polarized. The latter observation indicates that the effective symmetry of NiTP-B is more like that of NiOEC ($C_2'$) than NiMP or the nickel di-β-oxoporphyrins ($C_2''$).

Each of the β-oxoporphyrins, including the five isomeric di-β-oxoporphyrins, has a characteristic RR spectrum. The position of the carbonyl stretching mode is highest for DP-II, which is the β-oxoporphyrin structure found in heme $d_1$ of dissimilatory nitrite reductase.[8] The pyrrole rings of DP-II are apparently slightly less aromatic than those of the other oxoporphyrins, which should lead to a slightly more flexible β-oxoporphyrin ring in DP-II.

RR studies with isotopically labeled β-oxoporphyrins are necessary to confirm the assignments suggested herein. Once the assignments have been secured, structural effects of axial ligation, spin, and oxidation state can be analyzed by RR spectroscopy. This work should lead to a better understanding of the special properties of the β-oxoporphyrins and of the role of the β-dioxoporphyrin-II ring in heme $d_1$ of dissimilatory nitrite reductase.

**Acknowledgment.** We would like to express our appreciation to Prof. Thomas G. Spiro (Princeton University), Dr. Keith P. Madden (University of Notre Dame), Prof. William Bernhard (University of Rochester), Prof. James R. Kincaid (Marquette University), and Dr. Krzysztof Bajdor (Technical University of Wroclaw) for helpful discussions, and a reviewer for informative comments on the $Ni^{3+/2+}$ potential in chlorins. In addition, we would like to thank Prof. James R. Kincaid for the generous use of his laboratory to collect the HeCd-excited resonance Raman spectral data, Prof. A. Graham Lappin for the generous use of his Varian spectrophotometer, and Mr. John M. Marshall (John M. Marshall's, Inc., South Bend, IN) for the generous gift of two Burmese rubies for the EPR experiments. Acknowledgment is made to the donors of the Petroleum Research Fund, administered by the American Chemical Society, for support of this research.

**Registry No.** **1a**, 2683-82-1; **1b**, 24803-99-4; **1b**$^+$, 74876-13-4; **1b**$^{2+}$, 115120-42-8; **2a**, 74071-47-9; **2b**, 100762-96-7; **2b**$^+$, 100762-98-9; **2b**$^{2+}$, 100762-97-8; **3a**, 15341-26-1; **3b**, 136174-34-0; **3b**$^+$, 136174-39-5; **3b**$^{2+}$, 136201-57-5; **4a**, 72999-12-3; **4b**, 136174-33-9; **4b**$^+$, 136174-40-8; **4b**$^{2+}$, 136174-46-4; **5a**, 74083-82-2; **5b**, 136174-35-1; **5b**$^+$, 136174-41-9; **5b**$^{2+}$, 136174-47-5; **6a**, 15299-27-1; **6b**, 136174-36-2; **6b**$^+$, 136174-42-0; **6b**$^{2+}$, 136174-48-6; **7a**, 15299-28-2; **7b**, 136174-37-3; **7b**$^+$, 136174-43-1; **7b**$^{2+}$, 136174-49-7; **8a**, 23895-71-8; **8b**, 136174-38-4; **8b**$^+$, 136174-44-2; **8b**$^{2+}$, 136201-58-6; **9a**, 15341-27-2; **9b**, 136201-56-4; **9b**$^+$, 136174-45-3; **9b**$^{2+}$, 136174-50-0.

(43) (a) Andersson, L. A.; Loehr, T. M.; Sotiriou, C.; Wu, W.; Chang, C. K. *J. Am. Chem. Soc.* **1986**, *108*, 2908–2916. (b) Andersson, L. A.; Loehr, T. M.; Chang, C. K.; Mauk, A. G. *J. Am. Chem. Soc.* **1985**, *107*, 182–191.

(44) Han, S.; Madden, J. F.; Thompson, R. G.; Strauss, S. H.; Siegel, L. M.; Spiro, T. G. *Biochemistry* **1989**, *28*, 5461–5471.